Available online at www.sciencedirect.com
SCIENCE DIRECT
Journal of Molecular Catalysis A: Chemical 246 (2006) 223–230
JOURNAL OF MOLECULAR CATALYSIS A: CHEMICAL
www.elsevier.com/locate/molcata

Aerial oxidation of *p*-isopropyltoluene over manganese containing mesoporous MCM-41 and Al-MCM-41 molecular sieves

S. Vetrivel, A. Pandurangan *

Department of Chemistry, Anna University, Chennai 600025, India

Received 7 January 2005; received in revised form 30 September 2005; accepted 20 October 2005
Available online 15 December 2005

Abstract

The catalytic activity of MCM-41 after impregnation with manganese species was investigated. Si-MCM-41 and Al-MCM-41 (Si/Al = 99 and 158) were synthesized by hydrothermal method. The XRD analysis shows that aluminium incorporated MCM-41 retains the hexagonal structure. The higher *d*-spacing values of Al-MCM-41 catalysts than that of pure MCM-41 indicate the incorporation of aluminium into the framework. Manganese oxide impregnated MCM-41 and Al-MCM-41 catalysts were also prepared by wet method. Their structures were confirmed by XRD. The presence of Mn^{2+} was evident through DR UV–vis and ESR spectroscopy. The catalytic activity of the above catalysts was studied by vapour phase oxidation of *p*-isopropyltoluene (*p*-cymene) with CO_2-free air in the temperature ranging from 200–400 °C. On comparison, the Mn-MCM-41 catalyst significantly shows higher *p*-cymene conversion and products selectivity. The major products were 4-methylacetophenone, 4-isopropylbenzaldehyde, 1,2-epoxyisopropylbenzaldehyde and 4-methylstyrene. Among the products, selectivity to 4-methylacetophenone was found to be higher than others. Activities of the catalysts follow the order Mn-MCM-41 > Mn-AlMCM-41 (99) > Mn-AlMCM-41 (158). Reaction conditions were optimized on better conversion and products selectivity and the results are discussed.

Keywords: Mn-MCM-41; DRS-UV; ESR; Oxidation; *p*-Cymene

1. Introduction

Oxidation reactions occupy a prominent place in both the science of catalysts and catalysis-based modern chemical industry [1,2]. Stoichiometric metal oxidants such as chromates and permanganate are widely used. An excessive quantity of toxic metals leads to the inevitable production of large amounts of toxic waste which in turn necessitate disposal. The recent research in the area of catalysis has concentrated on finding alternative methods that will increase yield and reduce waste [3]. It is evident that the use of air in place of other oxidants is clearly desirable on economic and environmental grounds. Oxidation of *p*-cymene is an industrially important reaction because of its 4-methylacetophenone product, which is used as a precursor for manufacture of perfumes and the other product of this reaction is 4-isopropylbenzaldehyde, which is also used as a flavoring agent for food materials [4]. Oxidation of *p*-cymene with manganese(III) porphyrin complex catalysts in the presence of hydrogen peroxide as the oxidant, using co-catalysts, like imidazole or ammonium acetate is already reported [5,6]. Aleksandrov and Basaeva et al. [7,8] reported the same reaction catalysed by Co and Mn complexes in acetic acid medium. Cerium(IV) ammonium nitrate in acetic acid to give nitro and acetate substituted derivatives [9] and oxides of Cr, Mn and Se have also been reported [10]. For the production of 4-isopropylbenzaldehyde, Vaudano and Tissot carried out the reaction in methanolic medium by direct electrochemical oxidation method [11]. Oxidation of *p*-methyltoluene and *p*-*tert*-butyltoluene catalysed by Co, Mn and NaBr salts in acetic acid medium and vapour phase oxidation of *p*-methoxy toluene over vanadium pentoxide based catalysts have also been reported [12–18]. Recently, Nair et al. [4] reported the aerial oxidation of substituted aromatic hydrocarbons catalysed by $Co/Mn/Br^-$ in water-dioxygen medium in the temperature range 383–423 K, in which, the *p*-isopropylbenzyl alcohol (54.7%) is more predominant than other products in the oxidation of *p*-cymene. In conventional methods acetic acid and methanol have been used as a solvents. Hence, in the present study, solvent free oxidation of *p*-cymene with CO_2-

* Corresponding author. Tel.: +91 44 22203158; fax: +91 44 22200660.
E-mail address: pandurangan_a@yahoo.com (A. Pandurangan).

1381-1169/$ – see front matter © 2005 Elsevier B.V. All rights reserved.
doi:10.1016/j.molcata.2005.10.024

free air over manganese oxide supported mesoporous MCM-41 molecular sieves at high temperature was carried out. MCM-41 catalysts have advantage of ease of recovery and recycling that are readily amenable to continuous processing. There is a considerable demand for large pore size catalyst for the synthesis of large molecules. This reaction is taken as a model to identify the potential of manganese impregnated MCM-41 catalyst for oxidation of industrially important compounds [19]. Further, conditions were optimised in order to attain higher substrate conversion and selectivity towards 4-methylacetophenone and 4-isopropylbenzaldehyde, which are commercially important products.

2. Experimental

2.1. Preparation of manganese impregnated catalysts

The parent MCM-41 and Al-MCM-41 catalysts were synthesized according to the previous reports [20–22] using $C_{16}H_{33}(CH_3)_3N^+Br^-$ as the template. 0.3 M manganese acetate solution was prepared and mixed with 3 g of MCM-41 or Al-MCM-41 under constant stirring. The solution was dried under reduced pressure, and calcined in air at 550 °C for 6 h.

2.2. Physicochemical characterization

The aluminium content in Al-MCM-41 was determined using ICP-AES with allied analytical ICAP 9000. The manganese content in Mn-MCM-41 and Mn-AlMCM-41 was estimated using AAS (GBC932 plus). The powder low angle XRD analysis was performed on a Scintag 2000 diffractometer equipped with liquid nitrogen-cooled germanium solid-state detector using Cu Kα radiation. ^{29}Si MAS-NMR spectra and were recorded on a DRX-500 FT-NMR spectrometer at a frequency of 59.64 MHz, at a spinning speed of 8 KHz with pulse length of 2.50 μs (45° pulse), delay time of 10 s and spectral width of 335 ppm. Two thousand scans were acquired with reference to trimethylsilylpropanesulphonic acid (TSP). The ^{27}Al MAS-NMR (MSL 400 spectrometer) spectra were recorded at a frequency of 104.22 MHz and at a spinning rate of 8 KHz with pulse length of 1.0 μs, with a delay time of 0.2 s, and a spectral width of 330 ppm. The total number of scans was 150 and the line broadening was 50 Hz. The ^{27}Al chemical shifts were reported in relation to the liquid solution of aluminium nitrate. The co-ordination environment of Mn-containing MCM-41 samples was examined by diffuse reflectance UV–vis spectroscopy. The spectra were recorded in Shimadzu UV-2101 spectrophotometer using in the wavelength range of 200–800 nm. The co-ordination environment of Mn in MCM-41 and Al-MCM-41 samples was further confirmed by X-band (9 GHz) ESR spectra were recorded at liquid nitrogen temperature on Varian E112 spectrometer. The relative ESR intensities were calculated by double integration of the recorded ESR signal. DPPH was used as the reference to mark the *g*-value.

2.3. Catalytic studies on oxidation of p-cymene

The catalytic activity of manganese impregnated MCM-41 samples were carried out in a fixed bed continuous down flow quartz reactor under atmospheric pressure in the temperature range of 200–400 °C in steps of 50 °C. The reactor packed with 0.3 g of the catalyst was placed in a tubular furnace. The catalyst was activated in nitrogen atmosphere for 1 h followed by air for 5 h at 550 °C and then cooled under a nitrogen stream to the desired reaction temperature. The *p*-cymene was fed into the reactor using a syringe infusion pump at a predetermined flow rate. The oxidation of *p*-cymene was carried out and the products mixture was collected for a time interval of 1 h. The products were analyzed by gas chromatography Perkin-Elmer (Clarus 500 model) equipped with Flame Ionization Detector and elite 5 ms capillary column. The identification of products was also performed on a Shimadzu GC-MS-QP1000EX gas chromatograph–mass spectrometer. All the catalysts were regenerated by burning away the coke deposit by passing air at a temperature of 500 °C for 6 h. The same catalysts were used continuously to study the effect of various parameters, viz., temperature, weight hourly space velocity and time-on-stream.

3. Results and discussion

3.1. Elemental analysis

The ICP-AES values obtained for Al-MCM-41 catalysts. It can be seen that the Si/Al molar ratio of the sample is almost same as that of the gel composition. The manganese content of the materials was estimated by AAS and their results are given in Table 1.

3.2. Low angle XRD

The purity and structure of the MCM-41 materials were synthesized by the low-angle XRD. The XRD patterns of calcined and impregnated materials are shown in Fig. 1A and B. It can be observed that all the above materials exhibit a strong peak in the

Table 1
Elemental analysis and *g*-value (ESR) of MCM-41 catalysts

Samples	Si/Al	ICP	AAS-manganese content		*g*-Value of Mn
			Theoretical (ppm)	Experimental (ppm)	
Mn-MCM-41	–	–	4.119	3.960	2.0018
Mn-AlMCM-41 (99)	100	99	4.119	3.905	2.0005
Mn-AlMCM-41 (158)	150	158	4.119	3.628	2.0018

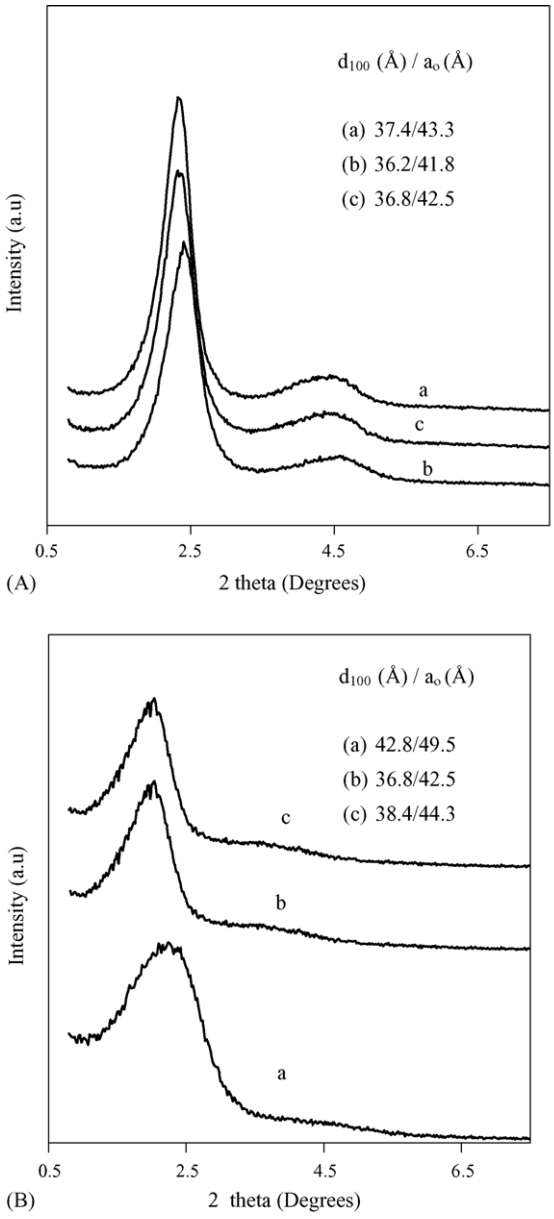

Fig. 1. XRD of (A) calcined (a) Si-MCM-41, (b) Al-MCM-41 (99), (c) Al-MCM-41 (158) and (B) after impregnation (a) Mn-MCM-41, (b) Mn-AlMCM-41 (99) and (c) Mn-Al MCM-41 (158).

2θ range of 1.9–2.4° due to 1 0 0 plane reflection lines. Additionally broad peaks at 2θ range of 3.6–4.5° are indicating the formation of well-ordered mesoporous materials. These peaks are generally indexed to the hexagonal regularity of MCM-41. The *d*-spacing values and hexagonal unit cell parameter (a_0) of MCM-41 are listed in same figure. The existence of the same peaks in the Al-MCM-41 as that of pure MCM-41 catalyst suggests that the long-range order is sustained even after the incorporation of aluminium. These peaks were broadened and shifted slightly to higher angle with increasing aluminium content, although the hexagonal structure still remained intact. These results suggest that the regularity of the mesoporous structure decreased and the pore size become slightly narrower with the incorporation of metals [21]. Further, during calcination, the

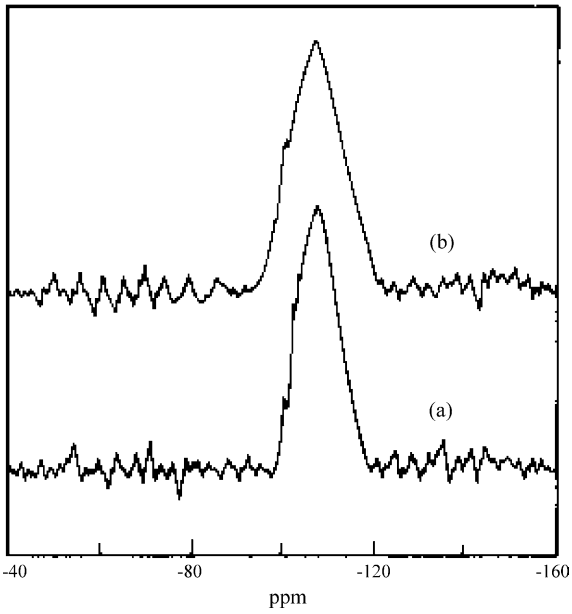

Fig. 2. ^{29}Si MAS-NMR spectra of calcined (a) Al-MCM-41 (99) and (b) Al-MCM-41 (158).

1 0 0 reflection shift to a higher value indicating a contraction of the lattice caused by template removal and subsequent condensation of silanol groups, which has been reported for MCM-41 materials [23]. The decrease in XRD signal intensity after calcination of MCM-41 is due to the saturation of the materials with air. Fig. 1B shows the XRD patterns of the manganese impregnated MCM-41 and Al-MCM-41 catalysts. Where intensity of the XRD patterns due to 1 0 0 plane decreased and that of 1 1 0 and 2 0 0 planes are disappeared owing to radiation diffusion [24].

3.3. ^{29}Si and ^{27}Al MAS-NMR spectroscopy

The co-ordination environment of silicon in hydrothermally synthesized mesoporous materials was analysed by ^{29}Si MAS-NMR spectroscopy and the spectra of calcined Al-MCM-41 (99 and 158) are shown in Fig. 2. The spectra show a broad signal at −110 ppm, which could be assigned to Si(OSi) and a shoulder at −103 to −108 ppm. The broadening in the lower field region can be assigned to silicon co-ordinated to aluminium. Considering the peak shift with Al co-ordination in alumino silicate zeolite, the most probable assignment of shoulders ranging between −103 and −108 ppm in the present case would be Si(OAl). These spectral features coined well with those reported by previous workers [25–27]. The ^{27}Al MAS-NMR spectra of the as-synthesized and calcined Al-MCM-41 (99) and Al-MCM-41 (158) are shown in Fig. 3. The spectra of the as-synthesized and calcined samples show a sharp resonance peak for tetrahedrally co-ordinated aluminium at $\delta = 53.0$ and 55.0 ppm, for Al-MCM-41 (99) and Al-MCM-41 (158), respectively, indicating that aluminium is tetrahedrally incorporated into the framework. The peak at $\delta = 0$ ppm, which corresponds to octahedral aluminium species, is not observed in the as-synthesized samples. But in the case of calcined samples, a

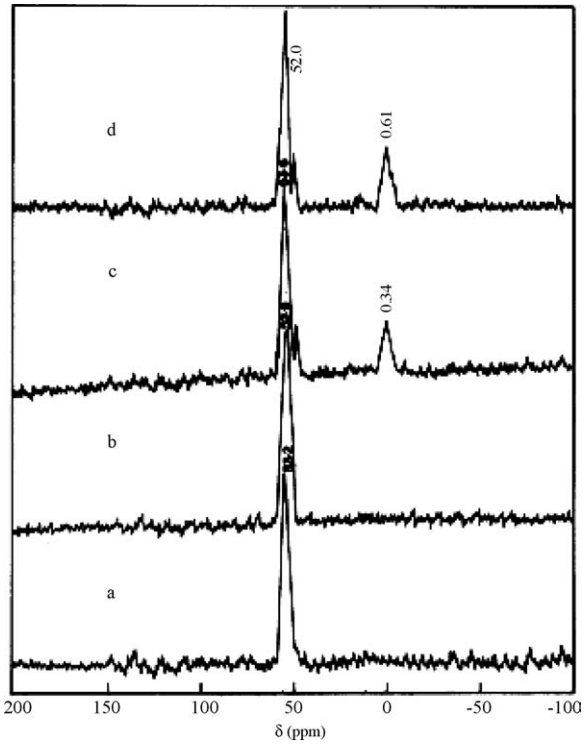

Fig. 3. ^{27}Al MAS-NMR spectra of as-synthesized (a) Al-MCM-41 (99), (b) Al-MCM-41 (158), calcined (c) Al-MCM-41 (99) and (d) Al-MCM-41 (158).

broad low intensity peak at $\delta = 0.3$ and 0.6 ppm for Al-MCM-41 (99) and Al-MCM-41 (158), respectively, indicating the presence of octahedral aluminium. The appearance of octahedral aluminium in calcined samples indicates that during calcination some aluminium species are removed from the framework. The ^{27}Al signals are found to be broader than the signals generally observed for zeolitic aluminium, presumably due to greater distortions in the tetrahedral environment [28].

3.4. DRS UV–vis spectroscopy

Fig. 4 shows the diffuse reflectance UV–vis spectra of Mn impregnated MCM-41 and Al-MCM-41 catalysts were carried out between 200 and 800 nm covering the entire ultra violet and visible region. Mn-MCM-41 and Mn-AlMCM-41 produce less resolved absorption band with maxima at 270 and 500 nm, respectively. These absorption maxima are coincided with the reports in the literature [29]. As Mn is in the non-framework, it is to have an octahedral environment of oxygen. As Mn is in +2 oxidation state shown by ESR spectroscopy, it is to have ^{6}S groundterm. As ^{6}S does not have crystal field components, the electronic excitations are forbidden, but there may be spin orbit interactions, as reported in the literature [30] with which some transitions may have allowance. The absorption bands are observed for the above materials, but they cannot be due to $^6A_{1g} \rightarrow {}^4T_{2g}$ and charge transfer transition as reported in the literature [31,32]. No obvious difference could be seen from UV–vis spectra between these MCM-41 and Al-MCM-41 samples, indicating that the sensitivities of the bands at 270 and 500 nm may be different, and thus the intensities of these bands

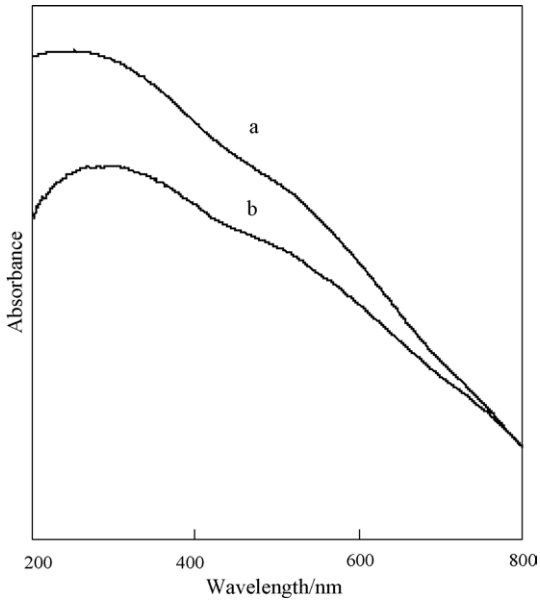

Fig. 4. DR UV-Vis spectra of calcined (a) Mn-MCM-41 and (b) Mn-AlMCM-41 (99).

cannot be used to evaluate the ratio of Mn^{2+}/Mn^{3+} in the samples [29].

3.5. ESR spectroscopy

A typical Mn(II) ESR spectrum is observed in manganese impregnated MCM-41 and Al-MCM-41 materials. Fig. 5 shows ESR spectra of calcined samples at liquid nitrogen temperature. Yonemitsu et al. [33] found a typical Mn^{2+} ESR signal from Mn-MCM-41 (Si/Mn = 20) and suggested that manganese existed as Mn^{2+} in their TIE sample. We observed X-band ESR spectra of the manganese impregnated MCM-41 and Al-MCM-41 samples. Where all the manganese containing samples shows the six hyperfine lines centered around $g = 2.00$ (Table 1) corresponding to Mn^{2+} in octahedral environment of oxygen. Similar observations were noted for Mn-MCM-41 [34] and MnAPO-5 [35] with the Mn species located at non-framework positions. The sextet lines are not equally spaced in both types of manganese impregnated MCM-41 and Al-MCM-41 samples. The splitting of the sextet increases from 3010 to 3550 G. Meanwhile, the line width and line height increases and decreases respectively from peak-to-peak. The average hyperfine coupling constant A_{iso} is 3280 G. These observations indicate that Mn(II) species in octahedral coordination, which is consistent with non-framework position [34,36].

3.6. Influence of temperature on p-cymene oxidation

The vapour phase oxidation of *p*-cymene was carried out over Mn-MCM-41 at 200, 250, 300, 350 and 400 °C. The flow rate of *p*-cymene WHSV was 3.3 h^{-1}. The flow rate of air was 50 ml/min. The major products were 4-methylacetophenone (4-MAP), 4-isopropylbenzaldehyde (4-IPB), 1,2-epoxyisopropylbenzaldehyde (1,2-EIPB) and 4-

Table 2
Products distribution of *p*-cymene oxidation over different catalysts at different reaction temperature

Catalysts	Temperature (°C)	Conversion (wt%)	Selectivity (%)				
			4-MAP	4-IPB	1,2-EIPB	4-MS	Others
Mn-MCM-41	200	43.8	37.6	5.8	6.8	42.3	7.5
	250	46.2	44.6	7.1	8.5	32.1	7.7
	300	55.2	52.8	10.0	11.5	15.4	10.3
	350	62.7	61.2	15.3	13.8	8.1	1.6
	400	51.5	55.3	26.4	15.3	2.1	0.9
Mn-AlMCM-41 (99)	200	39.0	39.0	6.1	7.7	42.0	5.2
	250	44.3	43.6	8.8	9.7	32.2	5.7
	300	48.8	51.2	10.9	12.6	17.7	7.6
	350	55.6	58.7	17.0	14.5	8.9	0.9
	400	41.5	53.0	28.4	17.0	1.6	–
Mn-AlMCM-41 (158)	200	37.6	36.4	8.0	8.1	40.3	7.2
	250	41.9	43.4	10.3	10.0	30.0	6.3
	300	47.9	49.0	14.4	14.0	15.1	7.5
	350	51.7	55.3	19.8	15.2	7.6	2.1
	400	43.1	48.0	31.3	17.6	3.1	–

Reaction condition: 0.3 g of catalyst; WHSV-3.3 h^{-1} and air 50 ml/min.

methylstyrene (4-MS). The small amount of 4-isopropylbenzyl alcohol and 4-isopropylbenzoic acid were obtained as by-products. These by-products were so small that the selectivity of major products was greater than 95% at the temperature 200 °C.

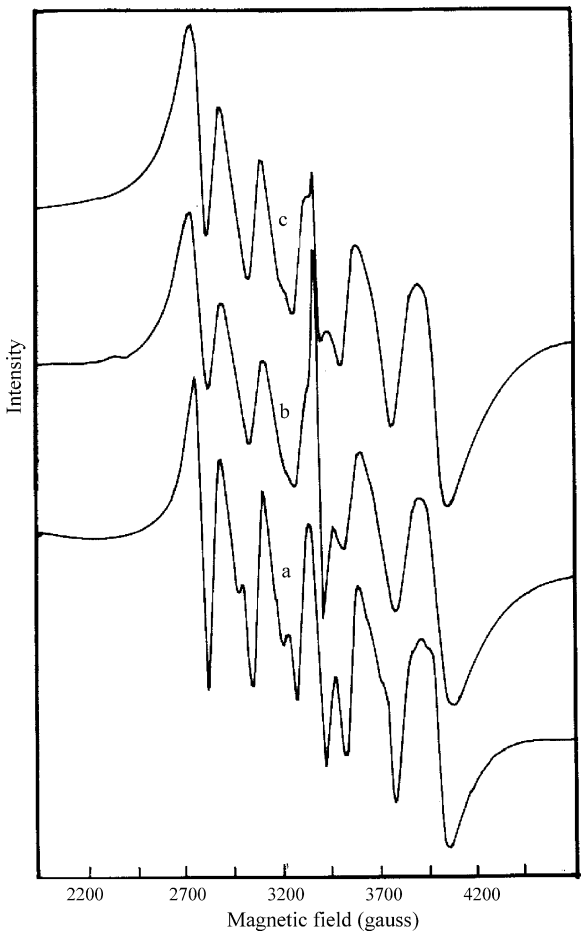

Fig. 5. ESR spectra of calcined (a) Mn-MCM-41, (b) Mn-AlMCM-41 (99) and (c) Mn-AlMCM-41 (158).

The *p*-cymene conversion and the products selectivity are presented in the Table 2. The *p*-cymene conversion increased with increase in temperature up to 350 °C, but at 400 °C it decreased. The decrease at the latter temperature is due to more amount of coke formation. Based on the products formed in this reaction, it is supposed that most of the manganese oxide particles may be in non-framework. The major product was observed to be 4-MAP whose selectivity increased with increase in temperature up to 350 °C, but at 400 °C it decreased. Formation of 4-MAP can be understood based on the following reaction Scheme 1.

Initially, Mn(II) species in the non-framework may be oxidized to Mn(IV) by oxygen [37]. There must be a simultaneous electron transfer to manganese and proton release from the tertiary hydrogen of *p*-cymene. The resulting free radical combines with oxygen to form superoxide. This superoxide abstracts a tertiary hydrogen atom from other *p*-cymene to yield hydroperoxide. This hydroperoxide decomposes thermally to yield 4-MAP and methanol. On other possibility is the superoxide may be converted to hydroperoxide by picking up an electron from Mn^{3+}

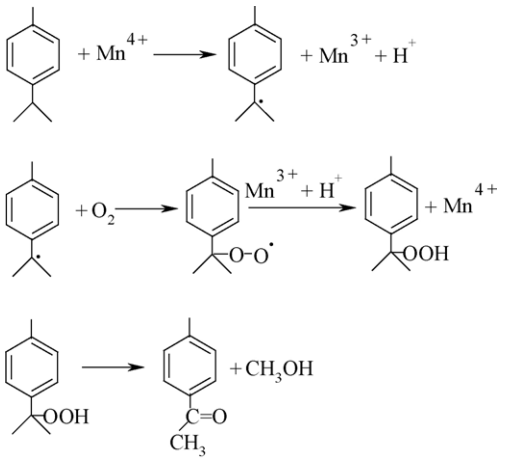

Scheme 1.

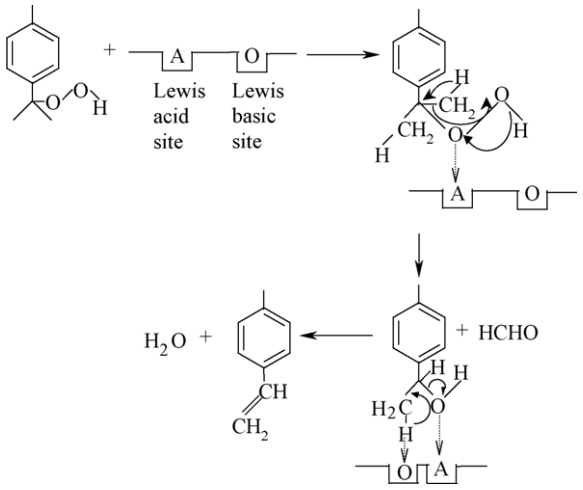

Scheme 2.

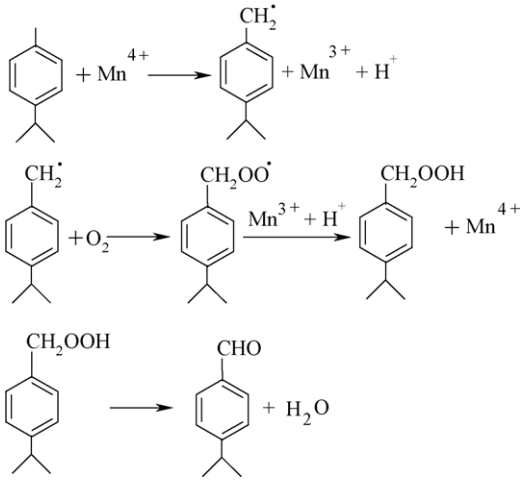

Scheme 3.

and combining with the already released H^+ as shown in the reaction Scheme 1. This route appears more appropriate than the previous one, as the role of Mn^{4+} is retained. The selectivity of 4-MAP, which is increased from 200 to 350 °C may be explained as follows. Since the decomposition of hydroperoxide is suggested to occur thermally, its formation alone is important. Therefore, the decrease at 400 °C might be attributed to partial blocking of active sites by coke.

The selectivity to 4-MS decreased with increase in temperature. The formation of 4-MS can be explained by the reaction Scheme 2 as shown below.

The hydroperoxide which thermally decomposes to give 4-MAP, can also be decomposed to yield 4-MS through complexation with the Lewis acid sites of the metal oxide particles. The hydroperoxide coordinates to the Lewis acid sites through oxygen adjacent to the alkyl group. This coordination activates the adjacent oxygen. This activated oxygen is added to one of the methyl groups in order to yield formaldehyde. The reorganization of atoms and bonds is illustrated clearly in the Scheme 2. Once formaldehyde is released, the resulting alcohol derivative undergoes dehydration over the same metal oxide particle to yield 4-MS. As the alcohol derivative is not observed in this reaction, either it must form freely and decompose instantaneously to give 4-MS or it may not be freely formed, so that the whole process of formation of formaldehyde and dehydration of 4-MS may be a single step process. The decrease in the selectivity of 4-MS with increase in temperature can be due to decrease the coordinated interaction of hydroperoxide with Lewis acid sites of the metal oxide particles.

The selectivity to 4-IPB increased with increase in temperature. The formation of 4-IPB is explained in the reaction Scheme 3. There is Mn^{4+} that abstract electron from methyl group of *p*-cymene to form free radical. Here, abstraction of electron from methyl group of *p*-cymene rather than isopropyl group is considered. The radical is stable, as there is a possibility of resonance. In the previous two reactions (Schemes 1 and 2), the abstraction of electron from the tertiary C–H bond is considered, but here the same from methyl hydrogen is considered. Based on this observation, it is suggested that tiny metal oxide particles can have varying degree of activity, as the size and surface free energy of them are different. The free radical reacts with molecular oxygen to produce superoxide, which then gets converted to peroxide, similar to reaction Scheme 1. The thermal decomposition of this peroxide is suggested to yield 4-IPB. Increase in selectivity with increase in temperature might be attributed to requirement of thermal energy for the decomposition of peroxide.

The selectivity to 1,2-EIPB increased with increase in temperature. The formation of this product is illustrated in the reaction Scheme 4.

Since, 1,2-EIPB is the precursor of the aldehyde the latter is suggested to react with Mn^{4+} of the metal oxide particles to yield the free radical. The free radical in turn reacts with molecular oxygen to produce superoxide. The latter species are converted to hydroperoxide similar to the previous reaction schemes. The thermal decomposition of hydroperoxide gives the 1,2-EIPB. A point to note is, though 1,2-EIPB is observed in this study, *p*-methyl-1,2-epoxyisopropyl benzene is not observed. Either this product would not have been formed in this study or would have

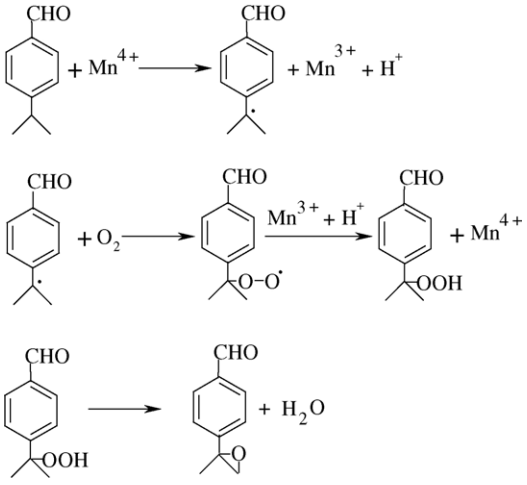

Scheme 4.

remained along with unidentified products. So the selectivity of 1,2-EIPB increased with increase in temperature. The increase might be due to high activation energy requirement for abstraction of hydrogen atom from the tertiary carbon. The presence of formyl group in the para position can also contribute to the increase in activation energy, as it is an electron-withdrawing group.

The results obtained with manganese oxide impregnated Al-MCM-41 (99) is presented in the same table. The data illustrate the same major products observed with Mn-MCM-41. Hence, there may not be any change in the major class of the reactions that occur over this catalyst. Comparison of conversion illustrates slightly less value for these catalysts than the former. The selectivity to 4-MAP increased from 200 to 350 °C, but at 400 °C it decreased. This trend is similar to that observed over Mn-MCM-41. The selectivity to 4-IPB, 1,2-EIPB and 4-MS also exhibits the same trend as Mn-MCM-41. Under the same condition, the reaction was also studied over manganese oxide impregnated Al-MCM-41 (158). The conversion and product selectivity exhibits a similar trend to that observed with manganese oxide impregnated AlMCM-41 (99) but compared to Mn-AlMCM-41 (99) catalysts, the Mn-AlMCM-41 (158) exhibits slightly low conversion and product selectivity. It might be due to more dispersion of manganese oxide particles because of high aluminium content in Al-MCM-41 (99), which leads to increase the density of acid sites. Further, it also evidenced from the AAS analysis.

3.7. Influence of weight hourly space velocity

The effect of WHSV over Mn-MCM-41 was studied at 3.3, 6.6, 10.3 and 13.3 h^{-1} at 350 °C. Conversion decreased as the WHSV increased. The selectivity to 4-MAP increased with increase in WHSV. Since *p*-cymene hydroperoxide is the common intermediate to form 4-MAP and 4-MS, based on the high selectivity of 4-MAP, it can be said that the decomposition route to 4-MAP would require less activation energy than the other route. In addition, the selectivity to 4-MS decreased with increase in the WHSV. The formation of this product becomes time dependent, thus, supporting our proposed reaction Scheme 2 involving coordination of hydroperoxide on the metal oxide particles to yield 4-MS. The selectivity to 4-IPB increased while the same to 1,2-EIPB increased with increase in WHSV. This observation clearly support that the formation of the latter product depends on the former.

The results obtained with manganese oxide impregnated Al-MCM-41 (99) catalyst shows the similar trend in conversion and products selectivity is observed as Mn-MCM-41. But the conversion is slightly less than Mn-MCM-41. In the case of manganese oxide impregnated Al-MCM-41 (158), conversion is still less than Mn-AlMCM-41 (99). The selectivity to 4-MAP increased with increase in WHSV and the values are almost close to Mn-AlMCM-41 (99). As observed with the previous catalyst, the selectivity to 1,2-EIPB increased and 4-IPB and 4-MS decreased with increase in WHSV. The results of WHSV studies are presented in Table 3.

3.8. Influence of time-on-stream

The effect of time-on-stream on conversion and products selectivity was examined over Mn-MCM-41 at 350 °C. The study was carried out for 5 h and the results are illustrated in Fig. 6. The conversion decreased with increase in stream due to coke formation, but the decrease is gradual. The coke was estimated after the end of time-on-stream study. It was found to be 18.9%. The selectivity to 4-MAP decreased while 4-MS increased with increase in stream. This observation illustrates the coordination of *p*-cymene hydroperoxide with manganese, which facilitates decomposition to 4-MS. Although formation of 4-MAP occurs via thermal degradation of *p*-cymene hydroperoxide, the probability for this hydroperoxide to coordinate with manganese is suggested to be high based on the high selectivity to 4-MS at the latter stage of stream. The selectivity to 4-IPB and 1,2-EIPB increased with increase in stream but the increase to latter is not much. The increase for latter is observed to be 9.9% at the end of 5 h of stream. This observation illustrates the formation of 1,2-EIPB on the more active sites.

Table 3
Products distribution of *p*-cymene oxidation over different catalysts at different WHSV

Catalysts	WHSV (h^{-1})	Conversion (wt%)	Selectivity (%)				
			4-MAP	4-IPB	1,2-EIPB	4-MS	Others
Mn-MCM-41	3.3	62.7	61.2	15.3	5.0	15.9	2.6
	6.7	55.2	64.4	16.0	4.4	13.1	2.1
	10.0	48.4	69.1	17.5	2.1	11.3	–
	13.3	39.0	71.8	19.0	1.1	8.1	–
Mn-AlMCM-41 (99)	3.3	55.6	58.7	17.0	6.0	16.7	1.6
	6.7	48.8	61.0	18.8	4.8	11.5	3.9
	10.0	44.1	63.6	20.0	2.9	9.4	4.1
	13.3	36.7	66.9	22.2	2.0	7.5	1.4
Mn-AlMCM-41 (158)	3.3	51.7	55.3	19.8	8.0	13.6	3.3
	6.7	45.4	60.1	21.1	5.5	10.0	3.3
	10.0	37.3	64.1	23.9	3.8	8.1	0.1
	13.3	34.4	65.9	25.0	2.5	6.6	–

Reaction condition: 0.3 g of catalyst, temperature 350 °C, and flow rate of air 50 ml/h.

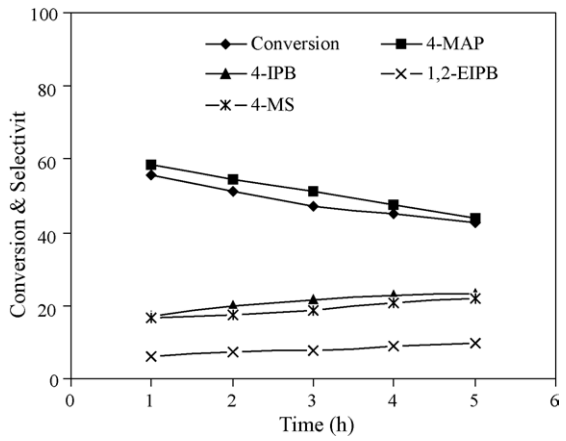

Fig. 6. Effect of time-on-stream on conversion and products selectivity over Mn-MCM-41.

4. Conclusion

The vapour phase oxidation of *p*-cymene with CO_2-free air was carried out over Mn-MCM-41, Mn-AlMCM-41 (99) and Mn-AlMCM-41 (158) yields 4-methylacetophenone, 4-isopropylbenzaldehyde, 1,2-epoxyisopropylbenzaldehyde and 4-methylstyrene as the major products. Conversion increased from 200 to 350 °C over all the catalysts, but decreased at 400 °C. Finely non-framework manganese oxide particles are observed to give high selectivity to 4-methylacetophenone at 350 °C. Again, Mn-MCM-41 is found to be more active than other manganese impregnated Al-MCM-41 catalysts due to its finely dispersed non-framework manganese oxide particles. The study of WHSV indicates that 3.3 h^{-1} is more favoured than other values. The time-on-stream study indicates a gradual decrease in conversion as well as 4-methylacetophenone selectivity with increase in stream. Where the decrease is attributed to coke formation. It could be concluded that Mn-impregnated MCM-41 and Al-MCM-41 catalysts are capable of effecting *p*-cymene conversion by forming 4-methylacetophenone as the major oxidized product. A suitable mechanism has been proposed, based on the products selectivity. The formation of 4-methylstyrene through metal coordination of *p*-cymene hydroperoxide is suggested in this study. The yield of 4-methylstyrene and 4-methylacetophenone depends on the formation of *p*-cymene hydroperoxide. The formation of 1,2-epoxyisopropylbenzaldehyde is shown to be dependent on the yield of 4-isopropylbenzaldehyde. Hence, this study illustrates that the manganese impregnated MCM-41 and Al-MCM-41 catalysts are sufficiently active for oxyfunctionalyzation of *p*-cymene.

References

[1] A. Bielanski, J. Haber, Oxygen in Catalysis, Marcel Dekker, New York, 1991.
[2] H.H. Kung, Transition Metal Oxides: Surface Chemistry and Catalysis, Elsevier, Amsterdam, 1989.
[3] R.A. Sheldon, Chem. Ind. (1997) 12.
[4] K. Nair, D.P. Sawant, G.V. Shanbhag, S.B. Halligudi, Catal. Commun. 5 (2004) 9.
[5] B. Meunier, Chem. Rev. 92 (1992) 1414.
[6] A. Thellend, P. Battiom, D. Mansuy, J. Chem. Soc., Chem. Commun. (1994) 1035.
[7] V.N. Alelsandrov, Zh. Org. Khim. 14 (7) (1978) 1517.
[8] N.N. Basaeva, T.A. Obukhova, R.P. Mironov, Osnovn. Org. Sint. Neftekhim 6 (1976) 11.
[9] E. Baciocchi, C. Rol, R. Ruzziconi, J. Chem. Res. Synop. 10 (1984) 334.
[10] N. Lijuan, J. Jinliang, Y. Zang, Jingxi Huagong 14 (4) (1997) 45.
[11] F. Vaudano, P. Tissot, Electrochim. Acta 46 (2001) 875.
[12] N. Shimizu, N. Saito, U. Michio, Stud. Surf. Sci. Catal. 44 (1989) 131.
[13] A.F. Kristi, US Patent US4740614.
[14] Ger. Offen, DE 3440407.
[15] G.H. Jones, J. Chem. Res. (S) (1982) 207.
[16] D.H.R. Barton, A.E. Martell, D.T. Sawyer (Eds.), The Activation of Dioxygen and Homogeneous Catalytic Oxidation, Plenum Press, New York, 1993.
[17] W. Partenheimer, J. Mol. Catal. 67 (1991) 35.
[18] S.A.H. Zaidi, Appl. Catal. 27 (1986) 99.
[19] P.A. Parikh, N. Subramanyam, Y.S. Bhat, A.B. Halgeri, Appl. Catal. A: Gen. 90 (1992) 1.
[20] R. Savidha, A. Pandurangan, Appl. Catal. A: Gen. 262 (2004) 1.
[21] M. Selvaraj, A. Pandurangan, K.S. Sehsdri, P.K. Sinha, V. Krishnasamy, K.B. Lal, J. Mol. Catal. A: Chem. 186 (2002) 173.
[22] J.S. Beck, J.C. Vartuli, W.J. Roth, M.E. Leonowicz, C.J. Kresge, K.D. Schmitt, C.T.W. Chu, D.H. Olson, E.W. Sheppard, S.B. McCullen, J.B. Higgins, J.L. Schlinker, J. Am. Chem. Soc. 114 (1992) 10834.
[23] C.T. Kresge, M.E. Leonowicz, W.T. Roth, J.C. Vartuli, J.S. Beck, Nature 359 (1992) 710.
[24] S. Vetrivel, A. Pandurangan, J. Mol. Catal. A: Chem. 227 (2005) 269.
[25] W. Kolodziejski, A. Corma, M.-T. Navarro, J. Perez-Pariente, Solid State Nucl. Magn. Reson. 2 (1993) 253.
[26] Y. Sun, Y. Yue, Z. Gao. Appl. Catal. A 161 (1997) 121.
[27] A. Matsumoto, H. Chen, K. Tsutsumi, M. Grun, K. Unger, Microporous Mesoporous Mater. 32 (1999) 55.
[28] K. Chaudhari, T.K. Das, A.J. Chandwadkar, S. Sivasankar, J. Catal. 189 (1999) 81.
[29] Q. Zhang, Y. Wang, S. Itsuki, T. Shishido, K. Takehira, J. Mol. Catal. A: Chem. 188 (2002) 189.
[30] F.A. Cotton, G. Wilkinson, Advanced Inorganic Chemistry, Wiley Eastern Private Limited, New Delhi, 1966.
[31] S. Velu, N. Shah, T.M. Jyothi, S. Sivasankar, Microporous Mesoporous Mater. 33 (1999) 61.
[32] F. Molella, J.M. Gallardo-Amores, M. Baldi, G. Busca, J. Mater. Chem. 8 (1998) 2525.
[33] M. Yonemitsu, Y. Tanaka, M. Iwamoto, Chem. Mater. 9 (1997) 2679.
[34] J. Xu, A. Luan, T. Wasowiscz, L. Kevan, Microporous Mesoporous Mater. 22 (1998) 179.
[35] Z. Levi, A.M. Raitsimring, D. Goldfrab, J. Phys. Chem. 95 (1991) 7830.
[36] S. Vetrivel, A. Pandurangan, Appl. Catal. A: Gen. 264 (2004) 243.
[37] L. Wang, J. Shi, J. Yu, D. Yan, Nanostruct. Mater. 10 (1998) 1289.